



Hollow fiber ultrafiltration membranes with microstructured inner skin

P.Z. Çulfaz^{a,c}, M. Wessling^{b,c}, R.G.H. Lammertink^{a,*}

^a Soft matter, Fluidics and Interfaces, Mesa+ Institute for Nanotechnology, University of Twente, Drienerlolaan 5, 7500AE Enschede, Netherlands

^b Chemical Process Engineering, AVT, RWTH Aachen University, Turmstr. 46, 52056 Aachen, Germany

^c Membrane Technology Group, University of Twente, Drienerlolaan 5, 7500AE Enschede, Netherlands

ARTICLE INFO

Article history:

Received 21 September 2010

Received in revised form 3 November 2010

Accepted 26 November 2010

Available online 3 December 2010

Keywords:

Hollow fiber

Microstructured bore

Corrugated membrane

Skin layer

ABSTRACT

Hollow fiber membranes with microstructured inner surfaces were fabricated from a PES/PVP blend using a spinneret with a microstructured needle. The effect of spinning parameters such as polymer dope flow rate, bore liquid flowrate, air gap and take-up speed on the microstructure and shape of the bore and its deformation was investigated. It was found that when a high bore liquid flowrate was used, the microstructure in the bore surface was destroyed. The bores were deformed to an oval shape when the fiber walls were thick. This was attributed to buckling of the fiber shell as a result of the coagulation and shrinkage of the outer surface. Fibers were also fabricated with a round-needled spinneret for comparison. The intrinsic pure water permeabilities (based on the actual bore surface areas) of fibers with structured and round bores were found to be similar. On the other hand, the structured fibers have larger pores in the skin layer. Smaller pores on the round fibers are considered to form when the inner surface coagulates and the skin layer is pulled inwards due to the shrinkage caused by phase separation. When the bore is structured, the wavy shape can damp this contraction effect resulting in larger pores. The skin layer thickness of the fibers was investigated using a colloidal filtration method. It was shown that fibers with microstructured bores which have mostly uniform skin layer thickness and reasonably narrow pore size distribution can be fabricated.

© 2010 Elsevier B.V. All rights reserved.

1. Introduction

Channels with microstructured surfaces are interesting for many applications. For asymmetric membranes, microstructuring the skin surface can enhance area-to-volume ratio and increase the productivity of the membrane [1–4]. Furthermore, the microstructure can create secondary flows that improve liquid mixing and therefore reduce concentration polarization [5–9]. Other applications include cell culturing for tissue engineering, where the microstructure or micropattern helps cell attachment and orientation [10–13], and microfluidic channels, where grooves on channel walls can improve mixing [14–16].

In the literature there are a number of studies illustrating that introducing corrugations that lie normal to the feed flow direction on flat sheet membranes can promote secondary flows and reduce concentration polarization [7–9,17,18]. Although microstructuring flat sheet membranes has been done more often, microstructuring tubular membranes is more rare. Broussous et al. reported the fabrication of ceramic tubular membranes with helical grooves on the inner surface. They observed significant flux improvement com-

pared to tubular membranes with smooth walls and attributed this improved fouling performance to the flow disturbance by the helical structure [5,6]. Ceramic microfiltration membranes with star-shaped channels are also commercially available [19,20].

Several researchers reported that when spinning hollow fiber membranes, under some conditions the bore becomes corrugated [21–25]. While this was mostly seen as an undesired irregularity in membrane research, for tissue engineering this phenomenon was exploited to fabricate porous fibers with well-aligned grooves which facilitate cell orientation in scaffolds [10,11,13].

Hollow fiber membranes with microstructured surfaces can also be fabricated using microstructured spinnerets. Fabrication of hollow fibers with microstructured outer surfaces has been reported for gas separation and ultrafiltration applications [1,3]. The spinneret used contains an insert with a microstructured hole in the middle, which transfers its shape to the membrane during phase separation. Nijdam et al. demonstrated that it is also possible to make fibers with microstructures on the bore side using a spinneret with a microstructured needle made by electroplating on an outside-structured fiber template [3].

In this study, we use a spinneret with a microstructured needle fabricated by laser ablation to make hollow fibers with microstructured bore for ultrafiltration applications. The parameters affecting the replication of the microstructure and deformation of the bore

* Corresponding author. Tel.: +31 53 4894798; fax: +31 53 4894611.

E-mail address: r.g.h.lammertink@utwente.nl (R.G.H. Lammertink).

Table 1
Fiber spinning parameters.

Fiber	Needle	Dope flowrate (ml/min)	Bore flowrate (ml/min)	Take-up speed (m/min)	Air gap (cm)	Residence time in air gap (s) ^a
SN1	Structured	5.35	1.76	4.0	11	1.7
SN2	Structured	2.28	1.76	4.0	11	2.3
SN3	Structured	2.28	1.76	2.0	11	3.6
SN4	Structured	2.28	1.76	4.0	5	1.1
SN5	Structured	5.35	1.76	4.0	35	5.2
SN6	Structured	5.35	1.76	8.0	35	3.5
SN7	Structured	5.35	1.76	8.0	11	1.1
SN8	Structured	5.35	2.81	4.0	11	1.6
SN9	Structured	2.28	2.81	4.0	11	2.3
RN1	Round	2.28	1.76	4.0	11	2.3
RN2	Round	2.28	2.81	4.0	35	7.2

^a To calculate the residence time in the air gap, the velocity in the air gap was estimated as the average of the polymer dope velocity exiting the spinneret and the take-up velocity.

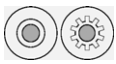
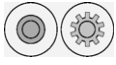

shape are investigated. The fibers were characterized with respect to permeability, pore size distribution and skin layer thickness and compared to round hollow fibers with inner skin.

2. Experimental

2.1. Fiber fabrication

The fibers were fabricated with the polymer dope 16.6% PES, 4.91% PVP K30, 4.91% PVP K90, 7.18% H₂O, 66.32% NMP. Water at room temperature was used as bore liquid. The external coagulation bath was water at 57 ± 5 °C. The spinning conditions for the fabrication of different fibers are summarized in Table 1. The spinneret used for fibers with microstructured bore is shown in Fig. 1. The needle was fabricated by laser ablation (Ligtmotif, Enschede-Netherlands). The dimensions of the microstructured spinneret and the round-needled spinneret used to spin round-bore fibers are given in Table 2.

Table 2
Spinneret dimensions.

		Microstructured spinneret	Round-bore spinneret
$A_{\text{needle,in}}$ (mm ²)		0.22	0.20
$A_{\text{needle,out}}$ (mm ²)		0.44	0.50
A_{dope} (mm ²)		1.33	1.27

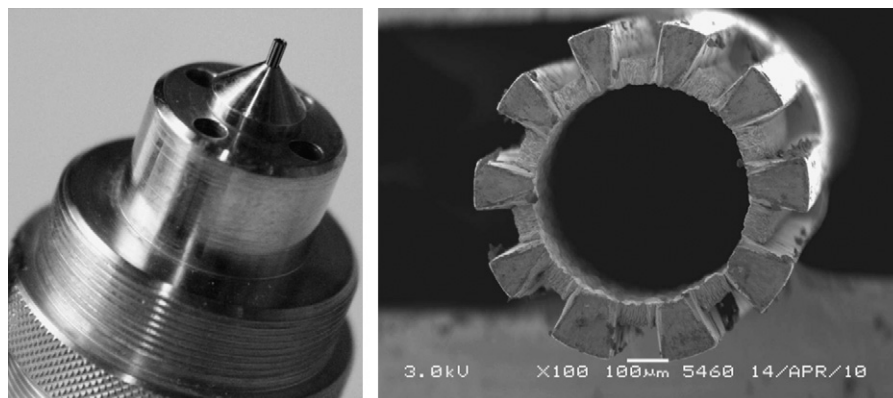
After spinning, the fibers were washed in water for 24 h. Then they were placed in 4000 ppm NaOCl solution for 48 h. After washing in water overnight, they were kept in 10% glycerol solution for 24 h and then dried under ambient atmosphere.

2.2. Fiber characterization

The morphology of the fibers was examined using Scanning Electron Microscopy (JEOL JSM 5600LV). The dimensions of the fibers were measured from the SEM images using ImageJ software.

The pure water permeabilities were measured using MilliQ water with 3-fiber modules of 20 cm length and under transmembrane pressure differences of 0.5 and 1.0 bar. Three modules were tested for each fiber batch. The permeabilities reported for the structured fibers were calculated using the actual convoluted surface area. In other words, the intrinsic permeabilities of the membranes, in units of L/h m² bar, are reported for both structured and round fibers.

The pore size distribution of the fibers was measured by permoporometry [1]. For skin layer thickness determination the colloidal gold filtration method was used [1]. Colloidal solutions of 20 nm gold particles were purchased from Sigma–Aldrich. Membrane modules of 3 cm² area (corresponding to single-fiber modules of ca. 10 cm) were prepared and 15 ml of 25 ppm gold solution was filtered from the shell side towards the bore under a transmembrane pressure difference of 1.5 bar. After filtration, the membranes were dried overnight in vacuum at 30 °C and fractured in liquid nitrogen. No further coating was applied on the cross section of the samples which were examined with the backscattered electron detector in the JEOL JSM 5600LV Scanning Electron Microscope under low vacuum (20–25 Pa).

**Fig. 1.** The spinneret and the microstructured needle.

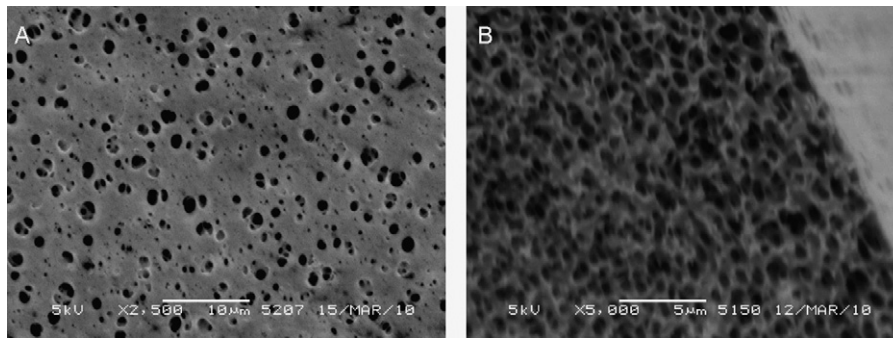


Fig. 2. The outer surface (a) and cross-section (b) of fiber SN2.

Table 3

Membrane area per fiber volume for fibers with structured and round bore as an indicator of surface area enhancement.

Fiber	Bore perimeter (mm)	Cross-sectional area (mm ²)	Membrane area per fiber volume (m ² /m ³)
SN1	2.90	1.33	2.18
SN2	2.53	0.95	2.67
SN5	2.67	1.34	1.99
SN6	2.60	1.26	2.06
SN7	2.65	1.22	2.18
RN1	2.15	0.93	2.31
RN2	2.09	0.90	2.31

3. Results and discussion

3.1. Fiber morphology

Fig. 2 shows the outer surface of fiber SN2. The outer surface of this fiber and all the other fibers are highly porous while the inner surfaces have a denser skin.

In Table 3, the inner perimeter and total cross-sectional area of the fibers with structured and round bores are given. The ratio of these two values, which is equivalent to the membrane area per

membrane volume, is shown in the last column. The structured-bore fiber SN2 has 16% higher membrane area-to-volume ratio than the round fiber RN1. The replication of the needle structure is similar for all structured fibers. Since the other four structured fibers (SN1, SN5, SN6 and SN7) shown in Table 3 have thicker walls, and therefore higher volume, the area-to-volume ratios are lower.

Among the fibers spun with the microstructured spinneret, different bore structures were observed. The fibers SN1, SN5, SN6 and SN7, shown in Fig. 3 were spun using the same dope and bore flowrates (Table 1). The fibers SN1 and SN7 were spun with an 11 cm air gap and take-up speeds of 4.0 and 8.0 m/min, respectively. SN5 was spun with a 35 cm air gap and take-up speed of 4.0 m/min, and SN6 was spun with a 35 cm air gap and take-up speed of 8.0 m/min. In all of these fibers, the microstructure of the bore is retained, however the bore shape is oval. In SN7, the bore is deformed the most and in SN5 the least. The bore of the fiber SN5 was observed to be round after spinning and even after a few hours of washing in water. The oval shape set in after the overnight washing.

On the bore of the fibers, coagulation starts the moment the dope and the bore liquid exit the spinneret. Then, when the fibers enter the water bath, the outer surfaces also coagulate. Although the vapor in the air gap can already initiate phase separation, it is in the water bath that phase separation on the outer surface is

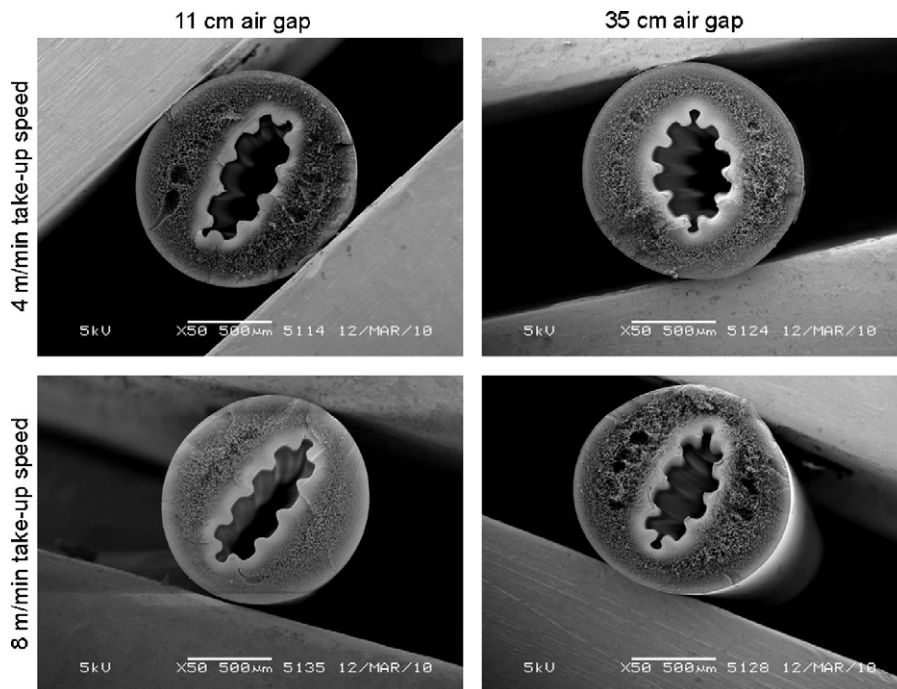


Fig. 3. Structured fibers SN1, SN5, SN6 and SN7 fabricated using a dope flowrate of 5.35 ml/min, a bore liquid flowrate of 1.76 ml/min with varying take-up speed or air gap.

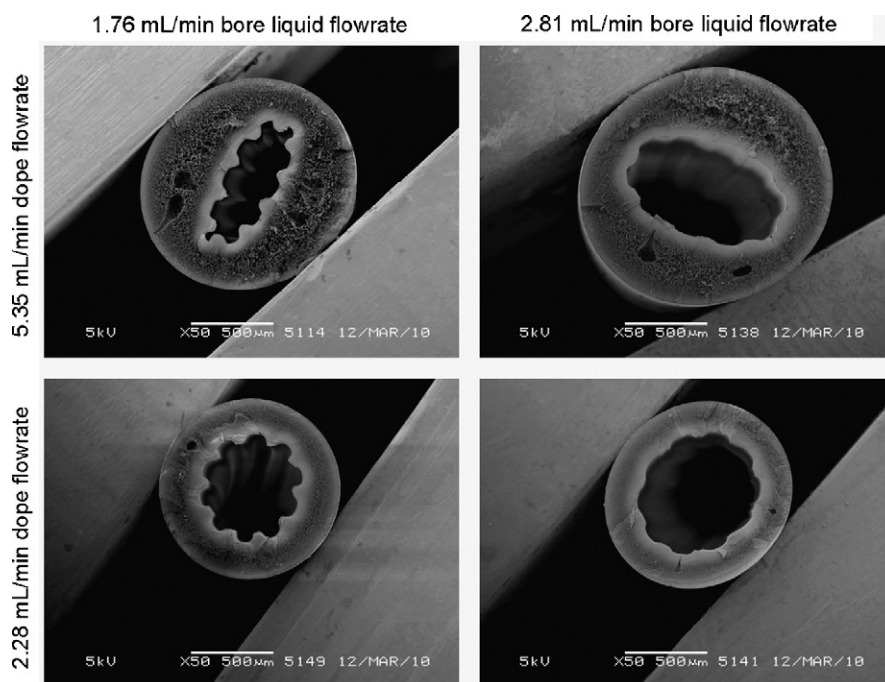


Fig. 4. Structured fibers SN1, SN2, SN8 and SN9 fabricated using a take-up speed of 4 m/min, air gap of 11 cm and varying dope or bore liquid flowrates.

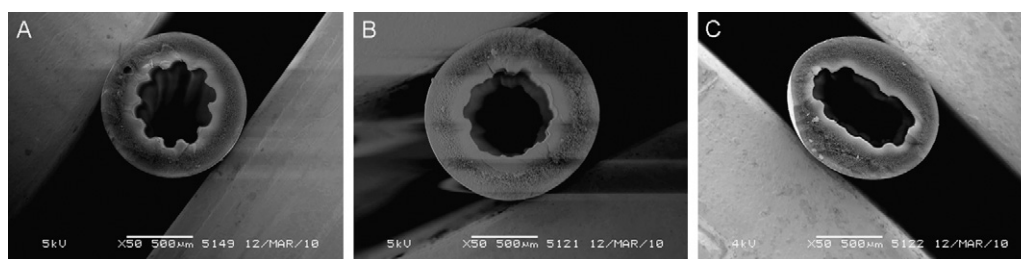


Fig. 5. Structured fibers SN2, SN3 and SN4 fabricated using a dope flowrate of 2.28 ml/min, a bore liquid flowrate of 1.76 ml/min and (a) 11 cm air gap, 4 m/min take-up speed, (b) 11 cm air gap, 2 m/min take-up speed and (c) 5 cm air gap, 4 m/min take-up speed.

complete. When the outer surface coagulates, it is pulled inwards due to the shrinkage after the solvent-nonsolvent exchange [26,27]. This pulling can deform the shape of the bore if the skin and the fiber shell are soft. A similar explanation was suggested by Bonyadi et al. who investigated the irregularity of fiber bores spun using a standard spinneret with a round needle [21]. They attributed the corrugations or irregularities in the bore to buckling of the elastic skin on the inner surface of the fibers. Among these four fibers, SN7 spends the least time in the air gap, and therefore by the time it enters the water bath, the skin formed on the inner surface of the

fiber is the softest and the polymer dope constituting the fiber shell is still of relatively low viscosity. There had been little time for non-solvent liquid induced phase separation from the inside and vapor induced phase separation from the outside. As a result, coagulation of the outer surface of the fiber deforms the bore of this fiber the most. For the fibers that spend more time in the air gap, the skin becomes more rigid, the polymer dope in the shell becomes more viscous and there is less deformation. The least deformation is seen in the fiber SN5, which spends the longest time in the air gap.

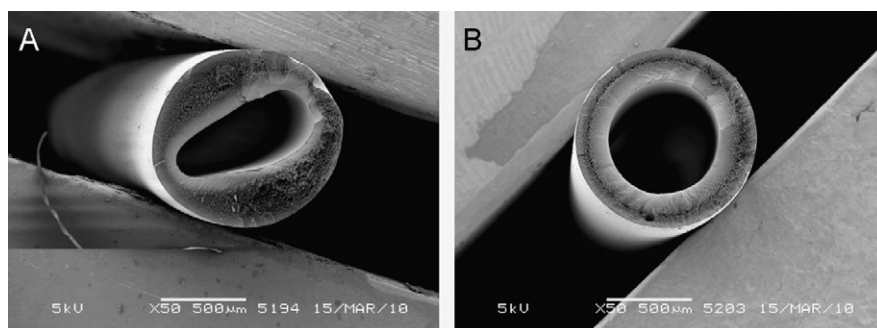


Fig. 6. The fibers RN1 (a) and RN2 (b).

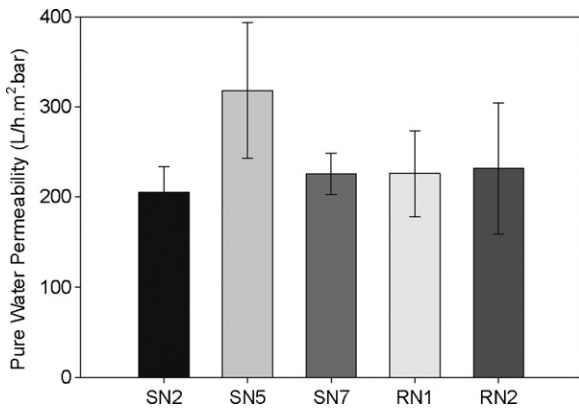


Fig. 7. Pure water permeability of fibers SN2, SN5, SN7, RN1 and RN2.

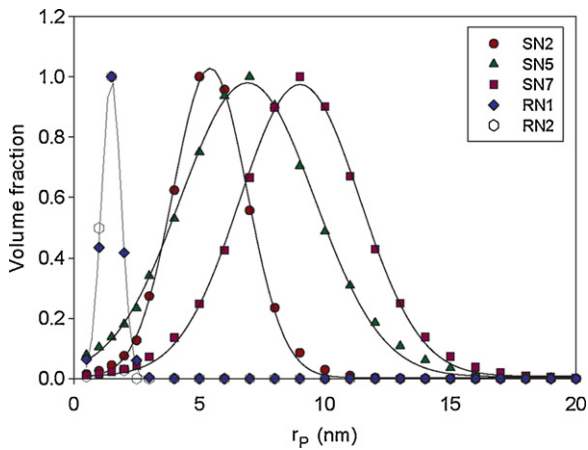


Fig. 8. Pore size distribution of fibers SN2, SN5, SN7, RN1 and RN2.

The fiber SN2 (Fig. 4) was spun with a lower dope flowrate than the fiber SN1 (Table 1) and the bore of this fiber is round, with the microstructure retained. The wall of the fiber is thinner and therefore by the time the fiber enters the water bath, the part of the shell that has undergone phase separation forms a higher fraction of the total. So when the outer surface coagulates, the shell is more viscous compared to SN1 and does not deform.

The fibers SN8 and SN9 were spun with a higher bore liquid flowrate than the fibers SN1 and SN2, respectively (Table 1, Fig. 4). The deformation of the bores are similar in SN1–SN8 (oval), and SN2–SN9 (round). However, for the fibers SN8 and SN9 spun with high bore flowrates, the microstructured shape of the bore is destroyed. A higher bore liquid flowrate exerts a higher pressure towards the outer radial direction. This pressure can destroy the structure before the skin can solidify and become rigid.

The fiber SN3 (Fig. 5(b)) was spun using a lower take-up speed than fiber SN2, with the rest of the spinning parameters the same

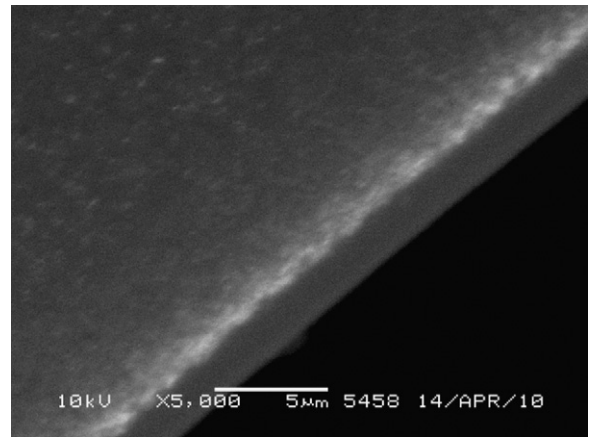


Fig. 10. Skin layer of fiber RN2.

(Table 1). The fiber has a thicker wall and the microstructure in the bore is destroyed although the overall shape is round. With a lower take-up speed there is expected to be more die swell, which can push the bore towards inside and destroy the microstructure [28].

The fiber SN4 (Fig. 5(c)) was spun using a lower air gap than fiber SN2, while the rest of the spinning parameters were kept the same (Table 1). With a short air gap of 5 cm, the skin can be so soft that it is both deformed to an oval shape and its microstructure is destroyed upon the coagulation of the outer surface.

In general, it was observed that a high bore liquid flowrate can destroy the microstructure on the inside surface. Also, when the skin on the inner surface of the fiber has not solidified to a certain extent, or when the fiber shell is still soft, the coagulation of the outer surface can deform the shape of the bore.

The fiber RN1 spun with the round needle with the same spinning parameters as the structured fiber SN2 has a deformed bore (Fig. 6). This implies that although the spinning conditions are the same, the phase separation process can be different for the fibers spun with the round and structured needle. The fiber RN2, spun using the round needle has a round bore and is used for further comparison with the structured fibers.

3.2. Fiber performance

The intrinsic pure water permeability of all the fibers is similar (Fig. 7). This indicates that the resistance of the skin layers should be comparable, since the skin forms the main contribution to the membrane resistance.

On the other hand, the mean pore sizes of the round fibers RN1 and RN2 are both lower than the structured fibers SN2, SN5 and SN7 (Fig. 8). The broadness of the pore size distributions is mostly similar. The full width at half maximum is $\pm 65\%$ of the mean for all fibers except for SN5, for which it is $\pm 85\%$ of the mean. The difference between the structured and the round fibers may be ascribed to the shrinkage of the polymer solution in the bore side upon coagu-

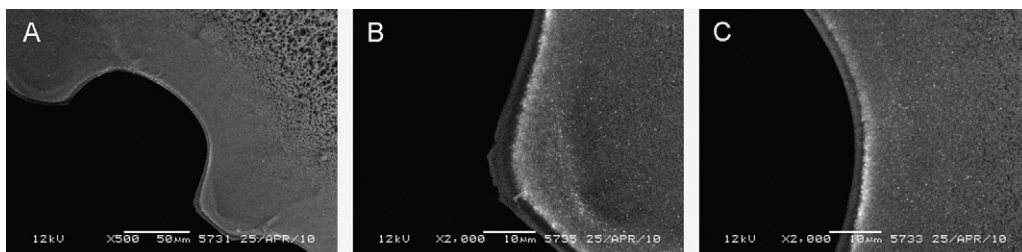


Fig. 9. Skin layer of fiber SN2: (a) one fin and groove, (b) corner of a fin and (c) corner of a groove.

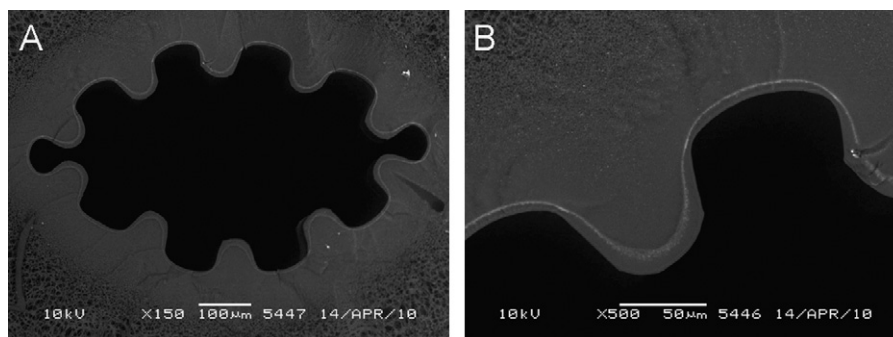


Fig. 11. Skin layer of fiber SN5: (a) full bore and (b) one fin and groove.

lation. When the polymer dope contacts the bore liquid and the skin is formed, the bore is pulled inwards due to the shrinkage caused by phase-separation [26,27]. When the bore is round, this pulling force can compress the pores being formed. However for a structured fiber, the wavy shape of the bore can damp the compressing effect of shrinkage.

Table 4 summarizes the skin layer thickness measured by the colloidal gold filtration method for a number of structured fibers and the round fiber RN2. Figs. 9–11 show the SEM pictures of the skin layers of the fibers SN2, RN2 and SN5 visualized by 20 nm gold particles.

For the structured fibers SN2 and SN7, the skin layer is 2 μm thick and this thickness is mostly constant throughout the surface. Only on the corner of the fins of SN2, it is locally thicker (Fig. 9(b)). The round fiber RN2 also has a skin layer of 2 μm (Fig. 10). On the other hand, for the fiber SN5, the skin is thickest on the top of the fins (9 μm) and gradually gets thinner towards the grooves (6 μm). In the corner of the grooves there is further thinning of the skin, where it becomes 3 μm (Fig. 11).

For the structured fibers with deformed bore shapes, the skin thicknesses are similar in all the grooves and fins. This supports the previous discussion that the deformation of the bore towards an oval shape happens due to the coagulation on the outer surface of the fibers, by which time the pore size in the skin should have mostly set in.

The thick skin layer of the fiber SN5 can be attributed to the thicker fiber wall caused by the high polymer dope flowrate used in spinning this fiber. Reuvers et al. who modelled the diffusion processes that occur after the immersion of a polymer solution in a nonsolvent bath predicted that the rate of diffusion in the coagulation bath and in the polymer solution is inversely proportional to the square of the initially cast film thickness [29]. From the moment the polymer solution is brought in contact with the nonsolvent bath until phase separation starts, a top layer with a high polymer concentration forms as a result of the solvent–nonsolvent exchange. With the onset of phase separation, this layer forms the skin of the membrane. For slower diffusion of the solvent and nonsolvent, the top layer has more time to grow and therefore is thicker. While this may offer an explanation to the thick skin layer of SN5, the fiber SN7 which has similar wall thickness, has a thinner skin layer. We must note that the skin layer thickness measured by the 20 nm gold col-

loids only indicates the location of the membrane where the pores are 20 nm in size. Considering that the mean pore diameter of the fiber SN5 is 14 nm and that of SN7 is 18 nm, and that both fibers have pores up to 30 nm in their skin layers (Fig. 8), the thickness measured from the SEM images should correspond to a location within the skin layer. Looking at the pore size distributions, a higher fraction of the skin layer of fiber SN7 has 20 nm pores compared to SN5, which can be the reason for the thinner “skin” measured with the gold colloids. In these fibers, the full skin layers, which have pores up to 30 nm size are then thicker than that outlined by the 20 nm colloids. The thick skin layers can explain why these fibers have comparable permeabilities as the round fibers, although they have larger pores.

For SN2 and RN2, the 20 nm colloids mark the full skin layer, since the pore size distributions in these fibers are 0–20 nm and 0–5 nm for SN2 and RN2, respectively. However, although the pore size distributions are different these fibers have comparable permeabilities. This implies that the porosity and/or pore connectivity is higher in the round fibers.

Among the structured fibers, only in SN5 the “skin” layer, or more correctly the location of 20-nm pores shows variations throughout the surface. In our previous studies with outside-structured fibers, we saw thinning of the skin layer locally in the corner of the grooves or gradual thinning from the fins towards the bottom of the grooves when we used polymer dopes of low coagulation value [1]. This thinning was attributed to the coagulant being enriched in solvent in the corner of the grooves due to the concave curvature. With the polymer dope used in the current study, which has 95% coagulation value, the variation in skin thickness was minimized. For outside structured fibers, the coagulation bath has constant composition since it is much larger than the fiber moving through it. For inside-structured fibers, the bore is continuously enriched in solvent until phase separation is complete. Parameters such as the size of the bore and the velocity profile in the bore liquid can strongly affect the coagulation conditions and as a result the rate and ratio of solvent and nonsolvent diffusion, and consequently the skin layer properties. For this reason, the coagulation processes can be different for inside and outside-skinned fibers although the same polymer dope and coagulant are used.

4. Conclusions

Fabrication of hollow fiber membranes with microstructured inner surfaces using a spinneret with a microstructured needle was reported. Fibers were spun using different polymer dope flow rate, bore liquid flowrate, air gap and take-up speeds. The effect of spinning parameters on the microstructure of the surface, the deformation of the bore and the permeability, pore size distribution and skin layer thickness of the fibers was investigated. It was observed that using a high bore liquid flowrate can destroy the

Table 4
Skin layer thickness of the fibers measured with 20 nm gold particles.

Fiber	Bottom of groove (μm)	Wall of groove (μm)	Top of fin (μm)	Corner of groove (μm)
SN2	2	2	2	2
SN5	6	–	9	3
SN7	2	2	2	2
RN2	2			

microstructure in the bore. When the skin on the inner surface of the fiber has not solidified to a certain extent, or when the fiber shell is still soft, the coagulation of the outer surface can deform the shape of the bore. This was attributed to buckling of the fiber shell as a result of the coagulation of the outer surface.

The intrinsic pure water permeabilities of fibers with structured and round bores were found to be similar. On the other hand, the pore size in the skin layer of the structured fibers was larger compared to the round fibers. Smaller pores on the round fibers are considered to form when the inner surface coagulates and the skin layer is pulled inwards due to the shrinkage caused by phase separation. When the bore is structured, the wavy shape can damp this contraction which may result in larger pores. The skin layer thickness of some of the structured fibers was observed to vary along the surface. This variation follows the same pattern observed with outside-structured fibers spun with low coagulation value polymer dopes. On the other hand, it was also shown that hollow fibers with microstructured bore can be fabricated with a uniform skin layer thickness and reasonably narrow pore size distribution. Under optimized spinning conditions, these fibers can be prepared such that they have enhanced membrane area-to-volume ratio, and therefore enhanced flow per module volume.

References

- [1] P. Çulfaz, E. Rolevink, C. van Rijn, R. Lammertink, M. Wessling, Microstructured hollow fibers for ultrafiltration, *Journal of Membrane Science* 347 (2009) 32–41.
- [2] A. Gronda, S. Buechel, E. Cussler, Mass transfer in corrugated membranes, *Journal of Membrane Science* 165 (2000) 177–187.
- [3] W. Nijdam, J. De Jong, C. Van Rijn, T. Visser, L. Versteeg, G. Kapantaidakis, G.-H. Koops, M. Wessling, High performance micro-engineered hollow fiber membranes by smart spinneret design, *Journal of Membrane Science* 256 (2005) 209–215.
- [4] A. Peters, R. Lammertink, M. Wessling, Comparing flat and micro-patterned surfaces: gas permeation and tensile stress measurements, *Journal of Membrane Science* 320 (2008) 173–178.
- [5] L. Broussous, J. Ruiz, A. Larbot, L. Cot, Stamped ceramic porous tubes for tangential filtration, *Separation and Purification Technology* 14 (1998) 53–57.
- [6] L. Broussous, P. Schmitz, H. Boisson, E. Prouzet, A. Larbot, Hydrodynamic aspects of filtration antifouling by helically corrugated membranes, *Chemical Engineering Science* 55 (2000) 5049–5057.
- [7] K. Scott, A. Mahmood, R. Jachuck, B. Hu, Intensified membrane filtration with corrugated membranes, *Journal of Membrane Science* 173 (2000) 1–16.
- [8] M. van der Waal, S. Stevanovic, I. Racz, Mass transfer in corrugated-plate membrane modules. II. Ultrafiltration experiments, *Journal of Membrane Science* 40 (1989) 261–275.
- [9] L.-Z. Zhang, Convective mass transport in cross-corrugated membrane exchangers, *Journal of Membrane Science* 260 (2005) 75–83.
- [10] A. Chwojnowski, C. Wojciechowski, K. Dudziski, E. Lukowska, Polysulphone and polyethersulphone hollow fiber membranes with developed inner surface as material for bio-medical applications, *Biocybernetics and Biomedical Engineering* 29 (2009) 47–59.
- [11] Y. Long, N. Zhang, Y. Huang, X. Wen, Formation of highly aligned grooves on inner surface of semipermeable hollow fiber membrane for directional axonal outgrowth, *Journal of Manufacturing Science and Engineering, Transactions of the ASME* 130 (2008) 0210111–0210118.
- [12] B. Papenburg, L. Vogelaar, L. Bolhuis-Versteeg, R. Lammertink, D. Stamatiadis, M. Wessling, One-step fabrication of porous micropatterned scaffolds to control cell behavior, *Biomaterials* 28 (2007) 1998–2009.
- [13] N. Zhang, C. Zhang, X. Wen, Fabrication of semipermeable hollow fiber membranes with highly aligned texture for nerve guidance, *Journal of Biomedical Materials Research-Part A* 75 (2005) 941–949.
- [14] M. Lopez, M. Graham, Enhancement of mixing and adsorption in microfluidic devices by shear-induced diffusion and topography-induced secondary flow, *Physics of Fluids* 20 (2008).
- [15] A. Stroock, S. Dertinger, A. Ajdari, I. Mezic, H. Stone, G. Whitesides, Chaotic mixer for microchannels, *Science* 295 (2002) 647–651.
- [16] A. Stroock, S. Dertinger, G. Whitesides, A. Ajdari, Patterning flows using grooved surfaces, *Analytical Chemistry* 74 (2002) 5306–5312.
- [17] J. Balster, M. Yildirim, D. Stamatiadis, R. Ibanez, R. Lammertink, V. Jordan, M. Wessling, Morphology and microtopology of cation-exchange polymers and the origin of the overlimiting current, *Journal of Physical Chemistry B* 111 (2007) 2152–2165.
- [18] N. Tzanetakis, K. Scott, W. Taama, R. Jachuck, Mass transfer characteristics of corrugated surfaces, *Applied Thermal Engineering* 24 (2004) 1865–1875.
- [19] T. Chiu, A. James, Critical flux determination of non-circular multi-channel ceramic membranes using TiO₂ suspensions, *Journal of Membrane Science* 254 (2005) 295–301.
- [20] F. Garcia, T. Chiu, Economic aspects of critical flux operability in star shaped microfiltration membranes: influence of some operating conditions, *Journal of Membrane Science* 325 (2008) 641–646.
- [21] S. Bonyadi, T. Chung, W. Krantz, Investigation of corrugation phenomenon in the inner contour of hollow fibers during the non-solvent induced phase-separation process, *Journal of Membrane Science* 299 (2007) 200–210.
- [22] J. van't Hoff, Wet spinning of polyethersulfone gas separation membranes, Ph.D. Thesis, University of Twente, 1988.
- [23] S. McKelvey, D. Clausi, W. Koros, A guide to establishing hollow fiber macroscopic properties for membrane applications, *Journal of Membrane Science* 124 (1997) 223–232.
- [24] Y. Santoso, T. Chung, K. Wang, M. Weber, The investigation of irregular inner skin morphology of hollow fiber membranes at high-speed spinning and the solutions to overcome it, *Journal of Membrane Science* 282 (2006) 383–392.
- [25] L. Shi, R. Wang, Y. Cao, C. Feng, D. Liang, J. Tay, Fabrication of poly(vinylidene fluoride-co-hexafluoropropylene) (PVDF-HFP) asymmetric microporous hollow fiber membranes, *Journal of Membrane Science* 305 (2007) 215–225.
- [26] M. Bikel, I. Punt, R. Lammertink, M. Wessling, Shrinkage effects during polymer phase separation on microfabricated molds, *Journal of Membrane Science* 347 (2009) 141–149.
- [27] A. Stropnik, V. Musil, M. Brumen, Polymeric membrane formation by wet-phase separation; turbidity and shrinkage phenomena as evidence for the elementary processes, *Polymer* 41 (2000) 9227–9237.
- [28] A. Ziabicki, *Fundamentals of Fibre Formation*, John Wiley & Sons, 1976.
- [29] A. Reuvers, C. Smolders, Formation of membranes by means of immersion precipitation. Part II. The mechanism of formation of membranes prepared from the system cellulose acetate–acetone–water, *Journal of Membrane Science* 34 (1987) 67–86.